J. Phys.: Condens. Matter **9** (1997) 8501–8514. Printed in the UK PII: S0953-8984(97)83623-5

Dynamical screening at the metal–semiconductor interface and excitonic superconductivity

Oleg Zakharov†, Marvin L Cohen†, Steven G Louie† and David R Penn‡

† Department of Physics, University of California at Berkeley, and Materials Sciences Division, Lawrence Berkeley National Laboratory, Berkeley, CA 94720, USA

‡ Electron and Optical Physics Division, Physics Laboratory, National Institute of Standards and Technology, Technology Administration, Department of Commerce, Gaithersburg, MD 20899, USA

Received 18 April 1997

Abstract. We examine the possibility of excitonic superconductivity at a metal–semiconductor interface. An *ab initio* RPA calculation of the screened Coulomb electron–electron interaction is performed for the silicon–jellium multilayer model. The superconducting kernel for this multilayered system is found to be positive in the whole frequency range considered. We show that the inclusion of local field effects does not change the sign of the kernel and thus does not enhance the excitonic mechanism.

1. Introduction

The BCS [1] theory of superconductivity is based on the concepts that electron pairing can lead to superconductivity and that the attractive pairing interaction which overcomes the Coulomb repulsion between electrons is caused by phonons. Earlier theories invoked a wide variety of mechanisms, but the successes of the BCS concepts inhibited the search for non-phonon mechanisms. Still suggestions appeared sporadically during 30 years between the publication of the BCS theory and the discovery [2] of high-T_c superconducting (HTS) oxides. During this period many of the suggestions relied on the pairing concept of BCS and speculated which bosons would replace phonons as the pairing mechanism. After the discovery of HTS oxides many of these mechanisms were resurrected and a number of new approaches were introduced.

Prior to the discovery of HTS oxides, one of the most popular suggestions for producing higher superconducting transition temperatures was the excitonic mechanism [3]. This mechanism was also resurrected by Bardeen *et al* [4] and others [5–7] as a possible explanation for high-temperature superconductivity in the oxides. However, here we will focus on the specific pairing mechanism; excitations of virtual electron–hole pairs. In particular, we will examine a more detailed model along the lines of the work of Allender, Bray and Bardeen (ABB) [8].

Although the mechanism is called excitonic, strictly speaking the virtual electron–hole pairs are not excitons since we do not consider bound electron–hole pairs. The contribution of electron–hole pairs to the dynamical screening can make the dielectric function negative in some frequency regions resulting in an attractive screened Coulomb interaction. It is important to note, however, that a negative dielectric function does not necessary yield pairing. The spatial or wavevector $\boldsymbol{q}$ dependence is of crucial importance. For example,

0953-8984/97/408501+14$19.50

a simple Drude dielectric function for a metal, $\epsilon(\omega) = 1 - \omega_p^2/\omega^2$, where ω_p is a plasma frequency, will yield negative values for $\omega < \omega_p$, but this will not lead to a superconducting electron plasma as demonstrated below by examining the BCS equation with a pairing interaction described in terms of a wavevector- and frequency-dependent dielectric function $\epsilon(\boldsymbol{q}, \omega)$.

Expressing the BCS equation in terms of an energy-dependent energy gap $\Delta(\varepsilon)$ and a kernel $K(\varepsilon, \varepsilon')$ yields

$$\Delta(\varepsilon) = -\int \frac{\Delta(\varepsilon')}{E'} K(\varepsilon, \varepsilon') \tanh\left(\frac{E'}{2k_B T}\right) \mathrm{d}\varepsilon' \tag{1}$$

where

$$K(\varepsilon, \varepsilon') \propto \int_{q_1}^{q_2} \frac{q\,\mathrm{d}q}{\epsilon(q, \omega)} \tag{2}$$

T is temperature, $E'^2 = \varepsilon'^2 + [\Delta(\varepsilon')]^2$, k_B is Boltzmann's constant, $\omega = \epsilon' - \epsilon$, and the integration limits q_1 and q_2 are determined by the condition of momentum conservation [9]. In the more general case of a crystalline solid with a non-homogeneous charge distribution, the kernel K is proportional to the average of the screened Coulomb interaction matrix elements between occupied states $|\boldsymbol{k}, \varepsilon_{\boldsymbol{k}}\rangle$ and unoccupied states $|\boldsymbol{k}', \varepsilon'_{\boldsymbol{k}}\rangle$.

The essential point concerning the negative regions of the dielectric function is that for a given ω, $\epsilon(\boldsymbol{q}, \omega)$ must be negative for a sufficient number of wavevectors $\boldsymbol{q}$ to give a negative value to the kernel K for this value of ω. A plasma model, or even a full $\epsilon(\boldsymbol{q}, \omega)$ modelled with the Lindhard dielectric function, will not produce a negative region sufficient to cause pairing [10].

To explore the excitonic mechanism with a detailed model, Allender, Bray and Bardeen (ABB) [8] used a Schottky barrier geometry with a metal in close contact with a semiconductor in order to allow electrons from the metal to penetrate into the semiconductor and pair via electron–hole-like excitations across the semiconductor gap. Instead of using a frequency dependent dielectric function to estimate K, ABB adopted a three-square-well model for K with phonon, Coulomb, and exciton kernels K_p, K_c, and K_e respectively having cutoff energies E_p, E_c, and E_e. Standard solutions for this model [8] were used as were solutions of the Eliashberg equations [11]. The conclusion reached was that if the usual estimates for K_p, K_c, E_p, and E_c are used along with ABB estimates for K_e and E_e, very large values of T_c are possible.

Estimates for K_e were made using a model proposed by Cohen and Anderson [12] for phonon interactions. The essential forms are

$$K_c - K_p = \frac{4\pi e^2}{Q^2 \epsilon(Q)}\left[1 - \frac{\Omega_p^2}{\epsilon(Q)\omega_{ph}^2(Q)}\right] \tag{3}$$

and

$$K_c - K_e = \frac{4\pi e^2}{Q^2 \epsilon(Q)}\left[1 - \beta\frac{\omega_p^2}{\epsilon(Q)\omega_g^2}\right] \tag{4}$$

where $\epsilon(Q)$ is the dielectric function for the wavevector Q, Ω_p and ω_p are the ionic and electronic plasma frequencies respectively, ω_{ph} and ω_g are the phonon frequencies and average gap energies, and β is a parameter which accounts for the time electrons from the metal spend in the semiconductor. Using estimates of β and characteristic ω_g values, ABB were able to estimate K_e. Because of the inverse dependence on ω_g, ABB suggested that narrow-gap semiconductors such as PbTe are preferable. Although tests were made

on Pb–PbTe systems, to our knowledge enhancements of T_c above that of Pb were not observed.

The next attempt to obtain an enhancement of T_c using a Schottky barrier was made by Inkson and Anderson (IA) [13] who suggested that ABB overcounted interactions. These authors considered analytic forms for the semiconductor and metal dielectric functions ϵ_s and ϵ_m based on simplified models. These dielectric functions had the form

$$\epsilon_s(q,\omega) = 1 + \frac{\epsilon_0 - 1}{1 + (q^2/\gamma^2)\epsilon_0 - (\omega^2/\omega_R^2)\epsilon_0} \tag{5}$$

where

$$\gamma^2 = k_s^2 \frac{\epsilon_0}{\epsilon_0 - 1}$$

and

$$\omega_R^2 = \omega_p^2 \frac{\epsilon_0}{\epsilon_0 - 1}.$$

Here ϵ_0 is the static electronic dielectric function, ω_p is the electronic plasma frequency, and k_s is the Fermi–Thomas screening wavevector. In the limit of $\omega \to 0$ and $q \to 0$, $\epsilon_s = \epsilon_0$.

The model dielectric function for the metal was expressed as

$$\epsilon_m(q,\omega) = 1 + \frac{1}{q^2/k_s^2 - \omega^2/\omega_p^2} \tag{6}$$

which gave the Drude and Fermi–Thomas limits correctly.

The IA argument can be simply expressed as follows. If we let

$$b = \frac{q^2}{\gamma^2} - \frac{\omega^2}{\omega_R^2}$$

then

$$\epsilon_m = 1 + \frac{\epsilon_0 - 1}{\epsilon_0 b}$$

and

$$\epsilon_s = 1 + \frac{\epsilon_0 - 1}{1 + \epsilon_0 b}.$$

Hence in the limit that $\epsilon_0 \to \infty$, $\epsilon_m = \epsilon_s$. For large ϵ_0, in the range of 20 to 100 for example,

$$\frac{1}{\epsilon_s} \approx \frac{1}{\epsilon_0} + \frac{\epsilon_0 - 1}{\epsilon_0 \epsilon_m}.$$

Since the pairing interaction in the semiconductor is proportional to $1/\epsilon_s$, IA argued that for large ϵ_0, which is expected for small-band-gap semiconductors, $1/\epsilon_s$ is essentially $1/\epsilon_m$ plus a positive term. The positive term will contribute a repulsive interaction to the pairing. Hence nothing is gained (and perhaps there is a loss) in the attractive interaction in forming the Schottky barrier. There is the added implication that ABB achieved an attractive contribution because of overcounting.

One weak point of the IA approach is the highly approximate forms of ϵ_s and ϵ_m. More rigorous calculations of the metal and semiconductor kernels were later performed by Cohen and Louie [10] who used the Lindhard dielectric function for the metal and a numerically calculated RPA dielectric function for Ge to estimate the superconducting kernels (2). In contrast to the kernels computed using the IA model dielectric functions, these kernels had no

attractive regions and were relatively insensitive to frequency. Based on the analogy with the electron–phonon interaction, the authors suggested that the local field effects [14, 15] which were not taken into account in their calculations can significantly change the character of the screened Coulomb interaction at the metal–semiconductor interface and, possibly result in the attractive region for the kernel for frequencies of the order of the semiconductor's fundamental gap.

Another criticism of the prior calculations of the Coulomb coupling at metal–semiconductor interfaces is the use of bulk metal and semiconductor dielectric functions. Charge redistribution at the interface can significantly affect screening in the physically interesting region within a few bond lengths from the interface. Also calculations [16] for metal–semiconductor interfaces revealed that electronic states near the Fermi surface of the metal would have characteristic features of the metal and the semiconductor near the interface. These states are called [16] metal-induced gap states (MIGSs). The MIGSs have density profiles which are constant in the metal and decay into the semiconductor with a decay length on the order of a bond length. Their energy position in the semiconductor is near the centre of the gap. In a sense the ABB parameter β is an empirical measure of this effect. It is these wavefunctions which should be considered when calculating pairing interactions due to the interface. In all previous calculations of the kernel the wavefunctions were assumed to be plane waves.

In this paper we address the issues described above. We present the results of an *ab initio* calculation of the dynamic dielectric matrix for a metal–semiconductor interface with local field effects included. We also estimate the energy-dependent superconducting kernel K using the calculated dielectric matrix and the calculated wavefunctions of the MIGS thus overcoming the limitations of the previous estimates of the kernel.

2. Method

We compute the RPA frequency-dependent dielectric matrix using the standard $\boldsymbol{q}$-space expression $\chi^0_{\boldsymbol{G}\boldsymbol{G}'}(\boldsymbol{q},\omega)$ [17] for the susceptibility of the non-interacting electron gas

$$\chi^0_{\boldsymbol{G}\boldsymbol{G}'}(\boldsymbol{q},\omega) = \frac{1}{\Omega}\sum_{\boldsymbol{k}}\sum_{n,n'}\frac{f_{\boldsymbol{k},n}-f_{\boldsymbol{k}+\boldsymbol{q},n'}}{\varepsilon_{\boldsymbol{k},n}-\varepsilon_{\boldsymbol{k}+\boldsymbol{q},n'}+\omega+\mathrm{i}\eta} \times\langle\boldsymbol{k},n|\,\mathrm{e}^{-\mathrm{i}(q+G)\cdot\boldsymbol{r}}|\boldsymbol{k}+\boldsymbol{q},n'\rangle\langle\boldsymbol{k}+\boldsymbol{q},n'|\,\mathrm{e}^{-\mathrm{i}(q+G')\cdot\boldsymbol{r}'}|\boldsymbol{k},n\rangle \tag{7}$$

where Ω denotes the crystal volume, n and n' are the band indices, $\boldsymbol{G}$ and $\boldsymbol{G}'$ are reciprocal lattice vectors, the sum over $\boldsymbol{k}$ runs over the Brillouin zone (BZ), $\{f_{\boldsymbol{k},n}\}$ are the occupation numbers, and η is a small positive number. The wavefunctions $|\boldsymbol{k},n\rangle$ and $|\boldsymbol{k}+\boldsymbol{q},n'\rangle$ and the eigenvalues $\varepsilon_{\boldsymbol{k},n}$ and $\varepsilon_{\boldsymbol{k}+\boldsymbol{q},n'}$ are obtained from the Local Density Approximation (LDA) calculation.

We construct ϵ^{RPA} from $\chi^0_{\boldsymbol{G}\boldsymbol{G}'}(\boldsymbol{q},\omega)$ using

$$\epsilon^{RPA}_{\boldsymbol{G}\boldsymbol{G}'}(\boldsymbol{q},\omega) = \delta_{\boldsymbol{G}\boldsymbol{G}'} - \chi^0_{\boldsymbol{G}\boldsymbol{G}'}(\boldsymbol{q},\omega)\frac{4\pi e^2}{|\boldsymbol{q}+\boldsymbol{G}'|^2}. \tag{8}$$

The off-diagonal elements of $\chi^0_{\boldsymbol{G}\boldsymbol{G}'}$ and $\epsilon^{RPA}_{\boldsymbol{G}\boldsymbol{G}'}$ have their origin in the non-homogeneous charge distribution for the solids. The non-diagonal contributions to the inverse of the macroscopic dielectric constant, $(\epsilon^{RPA})^{-1}_{00}$, are a consequence of local fields [17].

The screened Coulomb interaction V^{scr} between two electrons at $\boldsymbol{r}$ and $\boldsymbol{r}'$ can be

expressed as

$$V^{scr}(\boldsymbol{r},\boldsymbol{r}') = \frac{4\pi e^2}{\Omega}\sum_{\boldsymbol{q},\boldsymbol{G},\boldsymbol{G}'} \mathrm{e}^{\mathrm{i}(\boldsymbol{q}+\boldsymbol{G})\cdot\boldsymbol{r}}\frac{\epsilon^{-1}_{\boldsymbol{G}\boldsymbol{G}'}(\boldsymbol{q})}{|\boldsymbol{q}+\boldsymbol{G}'|^2}\mathrm{e}^{-\mathrm{i}(\boldsymbol{q}+\boldsymbol{G}')\cdot\boldsymbol{r}'}. \tag{9}$$

Here the sum over $\boldsymbol{q}$ runs over the first BZ. Because of local field effects, the Coulomb interaction between electrons in the crystal is non-local. If we neglect the local field contribution, the Coulomb interaction becomes local

$$V^{scr}(\boldsymbol{r}-\boldsymbol{r}') = \frac{4\pi e^2}{\Omega}\sum_{\boldsymbol{q},\boldsymbol{G}} \mathrm{e}^{\mathrm{i}(\boldsymbol{q}+\boldsymbol{G})\cdot(\boldsymbol{r}-\boldsymbol{r}')}\frac{1}{\epsilon_{\boldsymbol{G}\boldsymbol{G}}(\boldsymbol{q})}\frac{1}{|\boldsymbol{q}+\boldsymbol{G}|^2}. \tag{10}$$

To estimate the superconducting kernel K we need to compute matrix elements of the screened Coulomb potential V^{scr}

$$V_{\boldsymbol{k},\boldsymbol{k}'}(\varepsilon,\varepsilon') = \langle \boldsymbol{k}', -\boldsymbol{k}'; \varepsilon' | V^{scr} | \boldsymbol{k}, -\boldsymbol{k}; \varepsilon\rangle \tag{11}$$

corresponding to scattering of two electrons in the states $|\boldsymbol{k}\rangle$ and $|-\boldsymbol{k}\rangle$ with energy ε to the states $|\boldsymbol{k}'\rangle$ and $|-\boldsymbol{k}'\rangle$ with energy ε'.

The dimensionless kernel $K(\varepsilon,\varepsilon')$ is the average of the matrix element $V_{\boldsymbol{k},\boldsymbol{k}'}$,

$$K(\varepsilon,\varepsilon') = N(\varepsilon_{\boldsymbol{k}})\frac{\int\int \mathrm{d}\boldsymbol{k}\,\mathrm{d}\boldsymbol{k}'\, V_{\boldsymbol{k},\boldsymbol{k}'}\delta(\varepsilon-\varepsilon_{\boldsymbol{k}})\delta(\varepsilon'-\varepsilon_{\boldsymbol{k}'})}{\int \mathrm{d}\boldsymbol{k}\,\delta(\varepsilon-\varepsilon_{\boldsymbol{k}})\int \mathrm{d}\boldsymbol{k}'\,\delta(\varepsilon'-\varepsilon_{\boldsymbol{k}'})} \tag{12}$$

where $N(\varepsilon_{\boldsymbol{k}})$ is the density of states at $\varepsilon=\varepsilon_{\boldsymbol{k}}$.

If the states $|\boldsymbol{k},\varepsilon\rangle$ and $|\boldsymbol{k}',\varepsilon'\rangle$ are plane waves, the matrix elements are proportional to ϵ^{-1}

$$V_{\boldsymbol{k},\boldsymbol{k}'}(\varepsilon,\varepsilon') = \frac{4\pi e^2}{\Omega}\epsilon^{-1}_{\boldsymbol{G}\boldsymbol{G}}(\boldsymbol{q},\omega)\frac{1}{|\boldsymbol{q}+\boldsymbol{G}|^2} \tag{13}$$

where $\boldsymbol{k}'-\boldsymbol{k}=\boldsymbol{q}+\boldsymbol{G}$ and $\omega=\varepsilon'-\varepsilon$. In addition, if $\epsilon^{-1}(\boldsymbol{q},\omega)=\epsilon^{-1}(q,\omega)$, expression (12) reduces to (2).

For the more realistic case, $|\boldsymbol{k},\varepsilon\rangle$ and $|\boldsymbol{k}',\varepsilon'\rangle$ are the computed LDA Bloch wavefunctions

$$\begin{aligned}|\boldsymbol{k},\varepsilon\rangle &= \mathrm{e}^{-\mathrm{i}\boldsymbol{k}\cdot\boldsymbol{r}}\sum_{\boldsymbol{G}} c_{\boldsymbol{G}}\,\mathrm{e}^{\mathrm{i}\boldsymbol{G}\cdot\boldsymbol{r}}\\ |\boldsymbol{k}',\varepsilon\rangle &= \mathrm{e}^{-\mathrm{i}\boldsymbol{k}'\cdot\boldsymbol{r}}\sum_{\boldsymbol{G}} c'_{\boldsymbol{G}}\,\mathrm{e}^{\mathrm{i}\boldsymbol{G}\cdot\boldsymbol{r}}.\end{aligned} \tag{14}$$

Use of expression (9) for V^{scr} in momentum space gives

$$V_{\boldsymbol{k},\boldsymbol{k}'}(\varepsilon,\varepsilon') = \frac{4\pi e^2}{\Omega}\sum_{\boldsymbol{G},\boldsymbol{G}'} z^*_{\boldsymbol{G}}\frac{\epsilon^{-1}_{\boldsymbol{G}\boldsymbol{G}'}(\boldsymbol{k}'-\boldsymbol{k},\varepsilon'-\varepsilon)}{|\boldsymbol{k}'-\boldsymbol{k}+\boldsymbol{G}'|^2}z_{\boldsymbol{G}'} \tag{15}$$

where

$$z_{\boldsymbol{G}} = \sum_{\boldsymbol{G}'} c'_{\boldsymbol{G}+\boldsymbol{G}'}c^*_{\boldsymbol{G}'}.$$

3. Results and discussion

As a first approximation to the kernel K, we compute it assuming that the wavefunctions are plane waves

$$|\boldsymbol{k}\rangle = \frac{1}{\sqrt{\Omega}}\mathrm{e}^{-\mathrm{i}\boldsymbol{k}\cdot\boldsymbol{r}}. \tag{16}$$

We also assume that the Coulomb interaction is screened by the RPA dielectric function of Si.

We use a cutoff energy of 8 Ryd and include the contributions of 100 bands to compute the screening in Si. The computed RPA inverse dielectric function $\epsilon^{-1}(\omega)$ is presented in figure 1 for two different values of $\boldsymbol{q}$. The macroscopic inverse dielectric function with local field contributions is defined as $(\epsilon^{-1})_{00}$, where $\epsilon_{\boldsymbol{G}\boldsymbol{G}'}$ is the RPA dielectric matrix (8). The inverse dielectric function without local field contributions is $1/\epsilon_{00}$. From figure 1 we see that the local fields have almost no effect on ϵ for low frequencies. The screening with local fields is only slightly less effective (ϵ is smaller and ϵ^{-1} is larger) in this region. Around the plasma frequency, the local field effects become more important. The peak in the inverse dielectric function corresponding to the excitation of the plasmon is not as sharp if local fields are taken into account. This results in a less attractive negative region for ϵ^{-1}.

The frequency region where $\epsilon^{-1}(\omega)$ is negative shrinks with increasing q which is similar to the case of the Lindhard dielectric function. After a critical value of q (k_F for the Lindhard dielectric function), $\epsilon^{-1}(\omega)$ becomes positive everywhere.

To evaluate the integral in (2) $\epsilon^{-1}(\boldsymbol{q}, \omega)$ is computed on a 4:4:4 mesh in the BZ. When determining the integration limits q_1 and q_2, we assume the Fermi surface to be a sphere with a radius of 0.925 au^{-1} corresponding to a Fermi energy of 11.64 eV. The calculated values of K are presented in figure 2 as a function of frequency.

The frequency dependence of the kernel for silicon is in good agreement with the results of a similar calculation for germanium [16]. The kernel does not exhibit a strong variation with frequency. It has a minimum near the plasma frequency where the negative contribution from the low-q matrix elements is the largest but never becomes negative. The negative contributions for smaller-q matrix elements are compensated by the positive ones for larger q. The local field effects do not change the kernel significantly. Less efficient screening for the non-homogeneous charge distribution results in a larger K or stronger repulsion between the electrons when local fields are taken into account.

We now consider a more detailed model of a metal–semiconductor interface which provides us with a better approximation for the electron wavefunctions and screening at the interface. Our model consists of periodically spaced silicon slabs with jellium of density $r_S = 2.07$ in between them (see figure 3). Each slab contains six double layers of silicon atoms. The jellium layer is two silicon bond lengths (2×2.35 Å) thick.

We perform an LDA calculation with a cutoff energy of 6 Ryd and a 12:12:1 mesh of special $\boldsymbol{k}$ points in the BZ (19 $\boldsymbol{k}$ points in the irreducible wedge of the BZ) without relaxation of the positions of the silicon atoms. The computed LDA wavefunctions and eigenvalues are used to calculate the screening at the interface.

The system is metallic (with no gap) and exhibits a relatively low density of states at the Fermi energy (figure 4(a)). The density of states for the model considered is similar to the density of states of Si (figure 4(c)) except for MIGS in the gap. Even though we do not reconstruct the surfaces of the silicon slabs, the density of states does not exhibit sharp peak at the Fermi energy (figure 4(b)) corresponding to the dangling bond states which is typical for non-reconstructed semiconductor–vacuum interfaces.

The calculated total charge density for the metal–semiconductor interface model is shown in figure 5. The charge density inside a silicon slab is similar to that of bulk silicon. The remnants of dangling bonds at the silicon–jellium interface are visible in figure 5. The jellium density is close to the initial density (54 electrons/unit cell) but is no longer homogeneous as can be seen in figure 6.

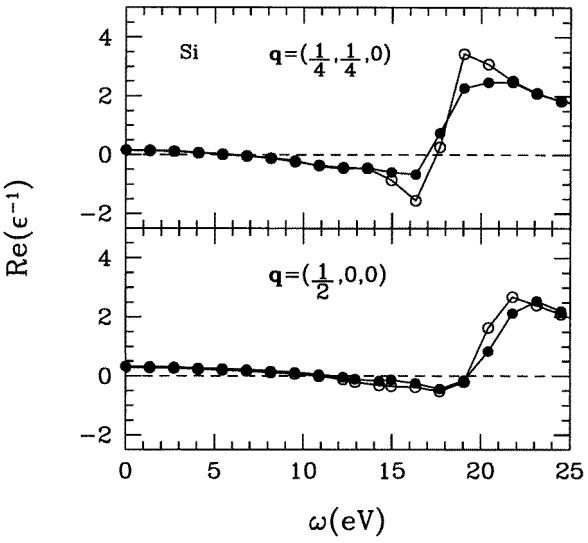

Figure 1. The calculated frequency-dependent RPA inverse dielectric function of Si for $\boldsymbol{q} = (\frac{1}{4}, \frac{1}{4}, 0)$ and $\boldsymbol{q} = (\frac{1}{2}, 0, 0)$ (in the reciprocal lattice basis). The solid (open) circles correspond to the inverse dielectric function with (without) the local field effects included. The lines are guides for the eye only.

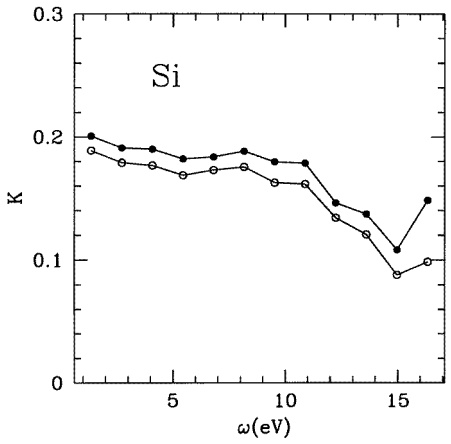

Figure 2. The calculated frequency-dependent superconducting kernel K for Si. The solid (open) circles correspond to the kernel computed with (without) local field effects included. The lines are guides for the eye only.

The plot of the one-dimensional total charge density along the z direction perpendicular to the layers is presented in figure 7. The dip in the jellium density indicates that there is a charge transfer from jellium into the semiconductor region.

We compute the frequency-dependent RPA inverse dielectric matrix for 15 different $\boldsymbol{q}$ vectors, and allow for 200 bands contributing to the sum over the bands in (7). The calculated inverse dielectric constant with and without local fields contributions is plotted in figure 8 as a function of frequency for two $\boldsymbol{q}$ vectors. The frequency dependence of the

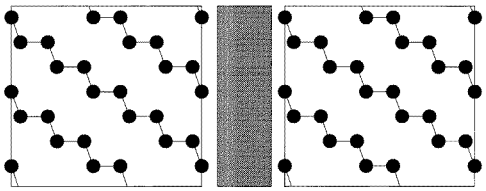

Figure 3. The geometry of the metal–Si interface model. The positions of the silicon atoms are represented by the solid circles. The shown cross-section corresponds to a (110) plane of bulk Si. The shaded area denotes jellium. Each silicon slab contains six double layers of silicon atoms. The width of the jellium layers is two silicon bond lengths. The distance between jellium and the closest plane of silicon atoms is half a bond length. The electron density of jellium is chosen to be equal to the electron density of Al ($r_S = 2.07$).

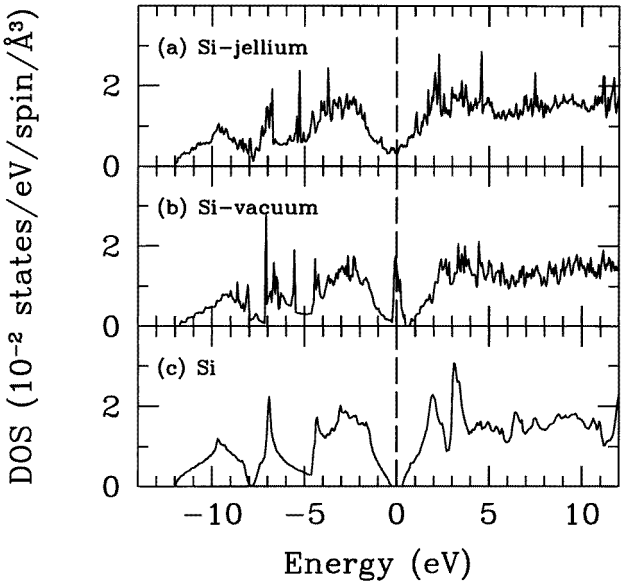

Figure 4. The calculated densities of states for Si–jellium (a) and Si–vacuum (b) multilayers and Si in the diamond structure (c). The zero of energy corresponds to the Fermi energy for (a) and (b), and to the middle of the gap for (c).

macroscopic inverse dielectric function is similar to the frequency dependence found for silicon (figure 1). As in the case of silicon local fields make the inverse dielectric constant less negative near the plasma frequency.

The MIGSs represent a rigorous quantum mechanical description of electron penetration from metal into semiconductor at a metal–semiconductor interface. Since we are interested in the possibility of Coulomb pairing by such electrons, we compute the superconducting kernel K for the Coulomb scattering of the MIGS pairs.

We choose two states with LDA energies close to the Fermi energy. The contour plots of the densities corresponding to these two states are shown in figure 9. Both of these states decay into silicon slabs since their energies lie in the bulk silicon gap. The state with $\boldsymbol{k} = (0, \frac{1}{3}, 0)$ has its maximum in the centre of the jellium slab whereas the state with $\boldsymbol{k} = (\frac{1}{12}, \frac{5}{12}, 0)$ bears some resemblance to the dangling bond states with the region of

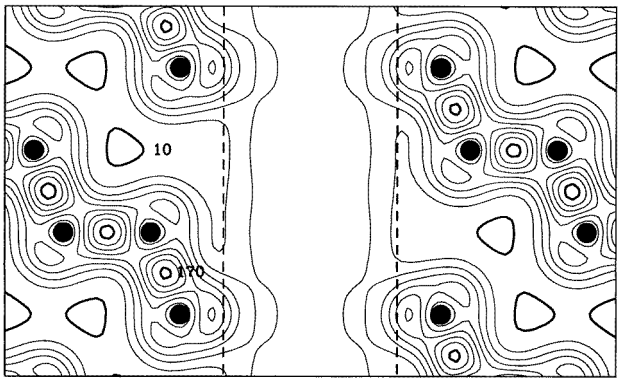

Figure 5. A contour plot of the calculated charge density for the Si–jellium multilayer. The shown cross-section corresponds to a (110) plane of bulk Si. The positions of the silicon atoms are shown by the solid circles. The thicker contours in the interstitial region regions correspond to the minimum charge density of 10 electrons/unit cell. The maximum charge density contours (170 electrons/unit cell) are in the bonds between the silicon atoms. The change in the charge density between the adjacent contours is 20 electrons/unit cell. The dashed lines correspond to the boundaries of the jellium layer.

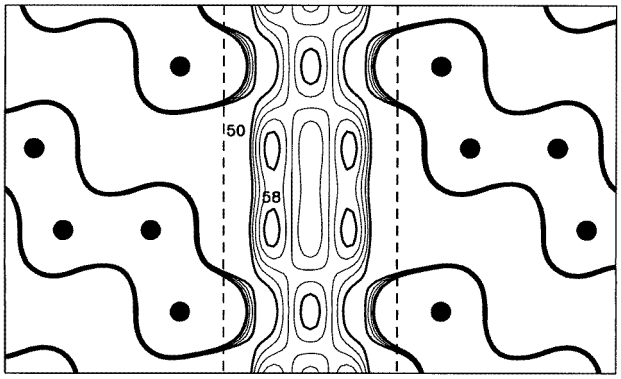

Figure 6. A contour plot of the calculated charge density for the Si–jellium multilayer. The contours corresponding to the values of the charge density between 50 and 58 electrons/unit cell are shown. The change in the charge density between the adjacent contours is 2 electrons/unit cell. The dashed lines correspond to the boundaries of the jellium layer.

maximum density being closer to the silicon atoms at the interface.

In figure 10 we show the matrix elements of the Coulomb scattering from these states with momentum transfer $\boldsymbol{q} = (\frac{1}{4}, 0, 0)$ and $\boldsymbol{q} = (\frac{7}{12}, \frac{1}{4}, 0)$. Even though the inverse dielectric function is negative for some frequency, the calculated matrix elements are always positive. This is a consequence of the fact that even without off-diagonal local field contributions, expression (15) for the matrix element includes contributions of diagonal elements $\epsilon^{-1}_{\boldsymbol{GG}}(\boldsymbol{q})$. These contributions are positive for all frequencies if $|\boldsymbol{G}|$ is large enough and they result in the overall positive value for the matrix element. The inclusion of the local field effects does not significantly change the matrix elements.

We estimate the superconducting kernel K by taking an average (12) of matrix elements over 15 different momentum transfer vectors $\boldsymbol{q}$. The calculated K (figure 11(a)) is always

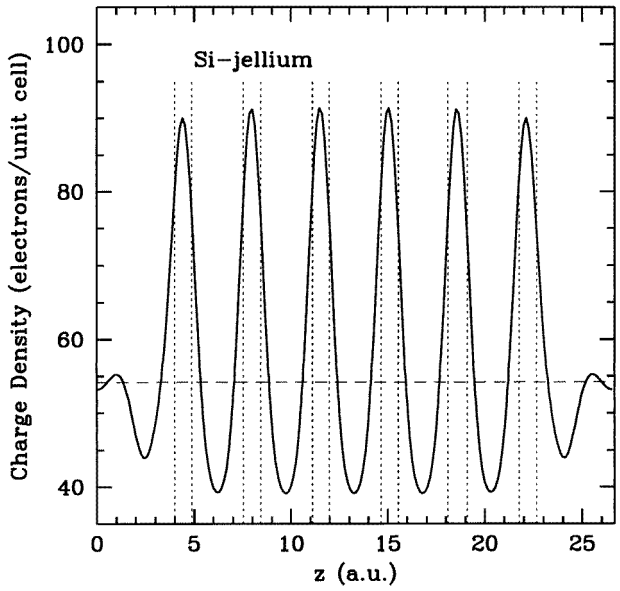

Figure 7. One-dimensional total charge density along the z direction. The dotted lines indicate the positions of the planes of silicon atoms. The broken line corresponds to the initial charge density of jellium.

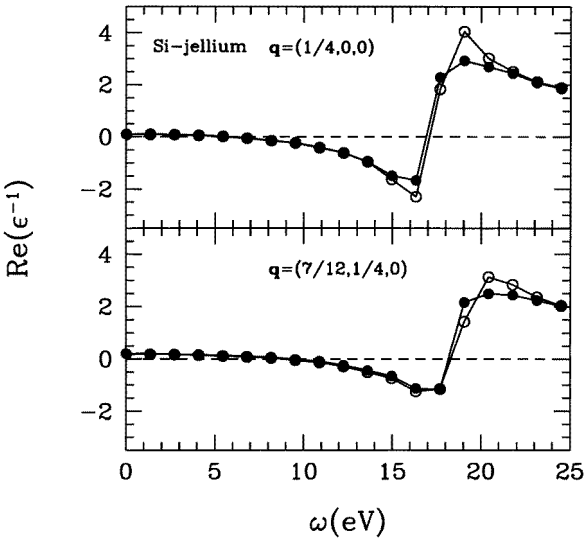

Figure 8. The calculated frequency-dependent RPA inverse dielectric function of the silicon–jellium multilayer for $\boldsymbol{q} = (\frac{1}{4}, 0, 0)$ and $\boldsymbol{q} = (\frac{7}{12}, \frac{1}{4}, 0)$ (in the reciprocal lattice basis). The solid (open) circles correspond to the inverse dielectric function with (without) the local field effects included. The lines are guides for the eye only.

positive as expected. It does not exhibit a strong frequency dependence except for a twofold increase at $\omega = 0$. The overall frequency dependence is similar to the one for the bulk

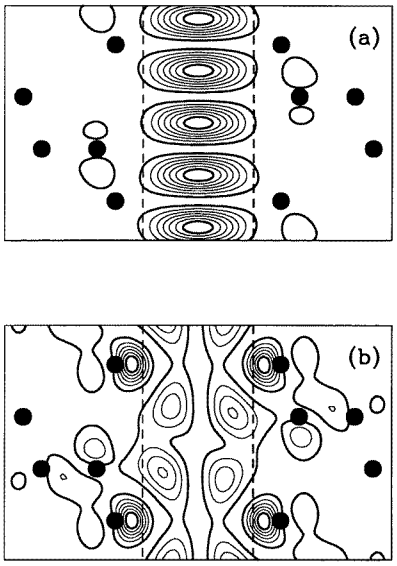

Figure 9. Contour plots of electron densities for two MIGS wavefunctions. Case (a) corresponds to the 30th band for $\boldsymbol{k} = (0, \frac{1}{3}, 0)$, case (b) corresponds to the 30th band for $\boldsymbol{k} = (\frac{1}{12}, \frac{5}{12}, 0)$. The dashed lines correspond to the boundaries of the jellium layer.

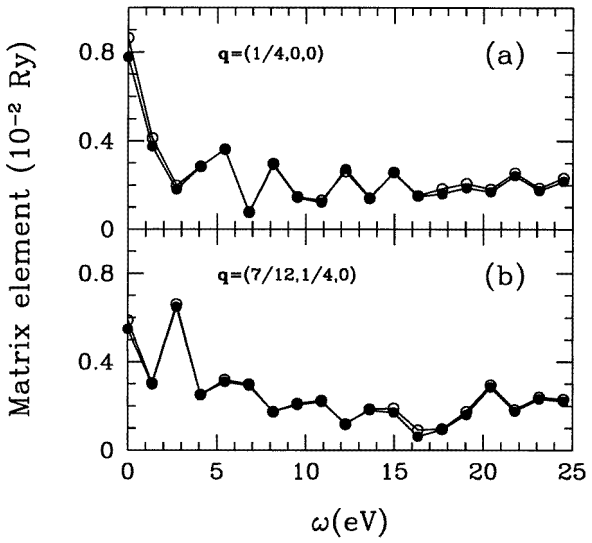

Figure 10. The calculated matrix elements for the Coulomb scattering of MIGS pairs with momentum transfer $\boldsymbol{q} = (\frac{1}{4}, 0, 0)$ (a) and $\boldsymbol{q} = (\frac{7}{12}, \frac{1}{4}, 0)$ (b). MIGSs are the Bloch states with $\boldsymbol{k} = (0, \frac{1}{3}, 0)$ (a) and $\boldsymbol{k} = (\frac{1}{12}, \frac{5}{12}, 0)$ (b). The solid (open) circles correspond to the matrix element computed with (without) the local field effects included. The lines are guides for the eye only.

silicon superconducting kernel (figure 2). The kernel with the local field effects included is slightly less repulsive than the kernel computed without local fields. This differs from the case of bulk silicon where the local field contributions result in larger positive values of the

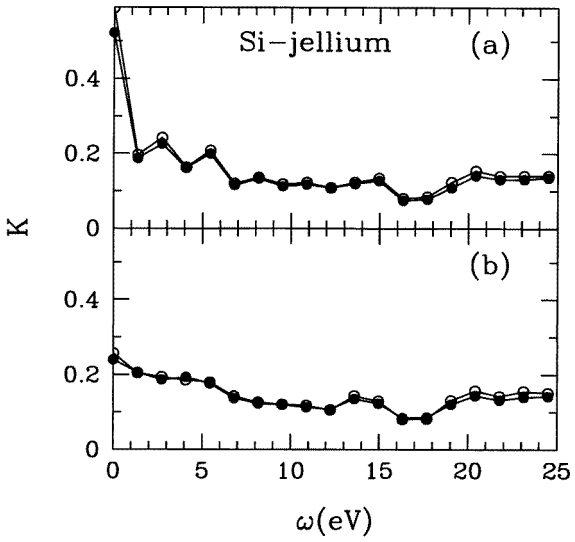

Figure 11. The superconducting kernel K as a function of frequency computed using the LDA wavefunctions (a) and wavefunctions modified to exclude the Coulomb interaction inside the jellium layer (b). The solid (open) circles correspond to the kernel computed with (without) the local field effects included. The lines are guides for the eye only.

kernel. This difference is explained by the fact that in the calculation for bulk silicon we assume the wavefunctions to be plane waves, and thus do not have the contribution of the ϵ^{-1} off-diagonal elements to the matrix elements. In our calculation of the kernel K for the silicon–jellium multilayer we use the LDA wavefunctions which are the sums of many plane waves. In this case the ϵ^{-1} off-diagonal elements contribute to the kernel, changing the sign of the effect.

Our calculations are performed for the particular geometry of the Si–jellium layers. One might argue that by changing the thickness of the jellium layer we can change the Coulomb matrix elements and consequently the superconducting kernel. Decreasing the width of the jellium layer is favourable from the point of view of excitonic superconductivity since the smaller the width the larger the fraction of time electrons from jellium spend in the interface region (or, in other words, parameter β of the ABB model will be larger). To study the effects of decreasing the width of the jellium layer without actually repeating costly calculations for a different geometry, we modify the LDA wavefunctions we use in the matrix element calculation by multiplying them in real space by a smooth function which is close to zero in the jellium layer and renormalizing them afterwards. The contour plots of two of these modified wavefunctions are given in figure 12.

The kernel K computed using such modified wavefunctions is shown in figure 11(b). This kernel differs significantly from the one computed with the LDA wavefunctions (figure 11(a)) only in the small-ω region. Comparing these two kernels we conclude that the increase of K at $\omega = 0$ was caused by the Coulomb repulsion in the jellium layer region. For the higher frequencies the kernel is almost unaffected by the modification of the wavefunctions. This result allows us to argue that the kernel will be positive for any geometry of the silicon–jellium interface.

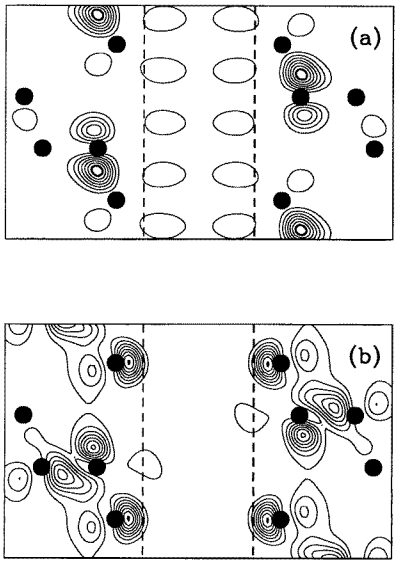

Figure 12. Contour plots of electron densities for two modified MIGS wavefunctions. The LDA wavefunctions shown in figure 9 are multiplied by the product of two Fermi factors which are close to zero in the jellium layer region. The dashed lines correspond to the boundaries of the jellium layer.

4. Conclusions

To examine the possibility of excitonic superconductivity at metal–semiconductor interfaces, we performed an *ab initio* calculation of the screened Coulomb electron–electron interaction for the silicon–jellium multilayer model. Our results are that within the RPA approximation for screening an attractive excitonic mechanism for electron pairing is not found. The superconducting kernel for this multilayered system is found to be positive in the whole frequency range considered. Its frequency dependence is similar to the frequency dependence for a bulk silicon superconducting kernel calculated using plane wave wavefunctions. We also show that changing the thickness of the metallic layer does not affect the frequency dependence of the kernel significantly. We find that the inclusion of local field effects results in very small changes in the kernel and thus does not enhance excitonic superconductivity.

Acknowledgments

This work was supported by National Science Foundation grant No DMR-9520554, and the Director, Office of Energy Research, Office of Basic Energy Services, Materials Sciences Division of the US Department of Energy under contract No DE-AC03-76SF00098. Computer time was provided by the NSF at the National Center for Supercomputing Applications.

References

[1] Bardeen J, Cooper L N and Schrieffer J R 1957 *Phys. Rev.* **108** 1175
[2] Bednorz J G and Müller K A 1986 *Z. Phys.* B **64** 189

[3] Ginzburg V L 1976 *Sov. Phys.–Usp.* **19** 174
[4] Bardeen J, Ginsberg D M and Salamon M B 1987 *Novel Superconductivity* ed S A Wolf and V Z Kresin (New York: Plenum) p 333
[5] Little W A 1987 *Novel Superconductivity* ed S A Wolf and V Z Kresin (New York: Plenum) p 341
[6] Varma C, Schimitt-Rink S and Abrahams E 1987 *Novel Superconductivity* ed S A Wolf and V Z Kresin (New York: Plenum) p 355
[7] Ginzburg V L 1987 *Priroda* **N7** 17 (in Russian)
[8] Allender D, Bray J and Bardeen J 1973 *Phys. Rev.* B **7** 1020
[9] Ihm J, Cohen M L and Tuan S F 1981 *Phys. Rev.* B **23** 3258
[10] Cohen M L and Louie S G 1976 *Superconductivity in d-and f-band Metals* ed D H Douglass (New York: Plenum) p 7
[11] Eliashberg G M 1960 *Sov. Phys.–JETP* **11** 696
[12] Cohen M L and Anderson P W 1972 *Superconductivity in d- and f-band Metals* ed D H Douglass (New York: AIP) p 17
[13] Inkson J C and Anderson P W 1973 *Phys. Rev.* B **8** 4429
[14] Adler S L 1962 *Phys. Rev.* **126** 413
[15] Wiser N 1963 *Phys. Rev.* **129** 62
[16] Louie S G and Cohen M L 1976 *Phys. Rev.* B **13** 2461
[17] Hybertsen M S and Louie S G 1987 *Phys. Rev.* B **35** 5585